small NANO MICRO

Drug delivery

Cellular Association and Assembly of a Multistage Delivery System

Rita E. Serda, Aaron Mack, Merlyn Pulikkathara, Ana Maria Zaske, Ciro Chiappini, Jean R. Fakhoury, Douglas Webb, Biana Godin, Jodie L. Conyers, Xue W. Liu, James A. Bankson, and Mauro Ferrari**

The realization that blood-borne delivery systems must overcome a multiplicity of biological barriers has led to the fabrication of a multistage delivery system (MDS) designed to temporally release successive stages of particles or agents to conquer sequential barriers, with the goal of enhancing delivery of therapeutic and diagnostic agents to the target site. In its simplest form, the MDS comprises stage-one porous silicon microparticles that function as carriers of second-stage nanoparticles. Cellular uptake of nontargeted discoidal silicon microparticles by macrophages is confirmed by electron and atomic force microscopy (AFM). Using superparamagnetic iron oxide nanoparticles (SPIONs) as a model of secondary nanoparticles, successful loading of the porous matrix of silicon microparticles is achieved, and retention of the nanoparticles is enhanced by aminosilylation of the loaded microparticles with 3-aminopropyltriethoxysilane. The impact of silane concentration and reaction time on the nature of the silane polymer on porous silicon is investigated by AFM and X-ray photoelectron microscopy. Tissue samples from mice intravenously administered the MDS support co-localization of silicon microparticles and SPIONs across various tissues with enhanced SPION release in spleen, compared to liver and lungs, and enhanced retention of SPIONs following silane capping of the MDS. Phantom models of the SPION-loaded MDS display negative contrast in magnetic resonance images. In addition to forming a cap over the silicon pores, the silane polymer provides free amines for antibody conjugation to the microparticles, with both VEGFR-2- and PECAM-specific antibodies leading to enhanced endothelial association. This study demonstrates the assembly and cellular association of a multiparticle delivery system that is biomolecularly targeted and has potential for applications in biological imaging.

Keywords:
- drug delivery
- imaging
- microparticles
- nanoparticles
- porous materials

[*] Prof. R. E. Serda, A. Mack, Dr. M. Pulikkathara, Dr. B. Godin, Prof. X. W. Liu, Prof. M. Ferrari
Department of Nanomedicine and Biomedical Engineering
University of Texas Health Science Center (UTHSC)
1825 Pressler St., Suite 537, Houston, TX 77030 (USA)
E-mail: Rita.Serda@uth.tmc.edu; Mauro.Ferrari@uth.tmc.edu

Dr. A. M. Zaske, Prof. J. L. Conyers
Center for Translational Injury Research
University of Texas Health Science Center (UTHSC)
6431 Fannin St., MSB 5.422, Houston, TX 77030 (USA)

Supporting Information is available on the WWW under http://www.small-journal.com or from the author.

DOI: 10.1002/smll.201000126

C. Chiappini, J. Fakhoury, Prof. J. A. Bankson
Department of Biomedical Engineering
University of Texas at Austin
1 University Station, C0400, Austin, TX 78712 (USA)

D. Webb, J. A. Bankson
Department of Imaging Physics
University of Texas M. D. Anderson Cancer Center
PO Box 301429, Houston, TX 77230 (USA)

M. Ferrari
Department of Experimental Therapeutics
University of Texas M. D. Anderson Cancer Center
Unit 422, 1515 Holcombe Blvd., Houston, TX 77030 (USA)

M. Ferrari
Department of Bioengineering
Rice University
Houston, TX 77005 (USA)

1. Introduction

While nanomedicine has made great strides in reaching the clinic with passively targeted liposomal doxorubicin[1–3] and taxane-loaded albumin nanoparticles,[4] custom-designed nanoparticles that specifically target pathological lesions are still in the developmental stages. Achieving site-specific delivery of therapeutics and contrast agents is the key to eliminating undesirable systemic effects and enhancing imaging and therapeutic efficacy. In addition to targeting cancer cells, blood-borne delivery systems must overcome abundant and sequential biological barriers. To overcome these challenges, we have envisioned a multistage delivery system (MDS) consisting of stage-one porous silicon microparticles (S1MPs) loaded with one or more types of second-stage nanoparticles that in turn carry either active agents or higher levels of nanoparticles.[5] Each level of complexity presents a solution for overcoming barriers, such as enzymatic degradation, negotiating vascular transport, crossing the vascular endothelium, and bypassing molecular efflux pumps. By employing methods of photolithography,[6,7] porous silicon microparticles have been fabricated with precise control over particle geometry and size, factors that govern vascular navigation, cellular uptake, and tissue distribution of the particles.[8–10] The tunable pore size of the S1MPs permits optimization of the MDS for specific loads,[6] as well as providing control over the rate of degradation.[11,12] The first level of targeting, which occurs in the blood vessel, is envisioned to be achieved at the level of the S1MP by attaching targeting moieties (e.g., peptides,[13] antibodies,[14] aptamers[15]) to the surface of the S1MP to direct interaction with tumor-associated endothelia lining the vessel wall.

One option for second-stage nanoparticles are superparamagnetic iron oxide (Fe_2O_3/Fe_3O_4) nanoparticles (SPIONs).[16,17] SPIONs are excellent contrast agents for magnetic resonance imaging (MRI).[14,18] Toxicity testing of SPIONs in animals,[19,20] and clinical use in humans,[21] supports their use as safe and well tolerated. Accumulation of nanoparticles inside a protective first-stage carrier may enhance the delivery of a large number of nanoparticles to a common destination, decrease renal elimination of small nanoparticles, and allow for temporal release of the second-stage particles. Additionally, transport in the silicon vector could potentially decrease the need for shielding of nanoparticles with polymers, such as polyethylene glycol (PEG),[22,23] and enhance retention of nanoparticle surface coatings and targeting ligands.

Herein, we examine cellular uptake of discoidal S1MPs by scanning electron microscopy (SEM), transmission electron microscopy (TEM), and atomic force microscopy (AFM). We present a biomolecularly targeted MDS comprising S1MPs encapsulating SPIONs within their porous matrix and examine intracellular localization of control and SPION-loaded S1MPs in macrophages. The effect of 3-aminopropyltriethoxysilane (APTES) modification of the porous silicon surface on both loading and retention of SPIONs is studied, with a detailed account of the effects of time and silane concentration on the extent of polymerization of the silicon surface. Additionally, free amines present in the silane polymer provide anchors for attaching functional units, and the impact of conjugating endothelial-specific antibodies to the MDS surface on cellular association is studied by confocal microscopy and flow cytometry. The potential for MRI with the MDS is examined by comparing spin and gradient echo relaxation times in phantoms containing either S1MPs or the MDS. Lastly, the in vivo stability of the MDS is studied by administration of the MDS to mice and staining of harvested tissues with Prussian blue.

2. Results

2.1. J774A.1 Macrophage Engulfment of S1MPs

Cellular engulfment of discoidal S1MPs by J774A.1 macrophages was demonstrated by SEM and AFM. The SEM images show unique J774A.1 cells at 10, 25, and 50 min after the introduction of S1MPs at 37 °C (Figure 1A). Cells were chosen as representative of the majority of cells at each time point and do not depict the kinetics of uptake of specific microparticles. Early time points show little, if any, extension of the cell membrane towards the microparticles. After 25 min, a cell is shown with one S1MP remaining on the cell surface, and a second S1MP completely covered by the cell membrane. At 50 min, a cell is shown with a partially internalized S1MP on the cell surface, while other microparticles may be completely internalized.

Confirmation of cellular uptake was obtained by imaging J774A.1 cells 1 h after introduction of S1MPs by AFM. Initial geometric analysis of S1MPs by AFM shows S1MPs with an aspect ratio of 6.4 based on a measured length of 3.9 μm and an average height of 0.605 μm (Figure 1B). An AFM image of a J774A.1 cell reveals a cell diameter of 21.5 μm, nucleus of 13.5 μm, and an internalized S1MP with a measured diameter of 3.2 μm (Figure 1C). Based on cellular topography, it is likely that multiple S1MPs are co-localized within the cell. These data support cellular uptake of discoidal S1MPs by macrophages.

2.2. Loading S1MPs with SPIONs

Discoidal S1MPs were fabricated by our group using standard photolithography and plasma etching. S1MPs with a diameter of 3.2 ± 0.2 μm (based on SEM analysis) and a pore size of 51.3 ± 28.7 nm were chosen to study the effect of silicon surface modification on loading of the porous matrix with secondary nanoparticles. SEM images were taken at increasing magnification to illustrate S1MP shape and relative pore size (Figure 2A). Ultrathin sections of S1MPs are also presented in TEM images in a series of increasing magnification (Figure 2B).

Loading of oxidized S1MPs with amine-modified 10 ± 2.5 nm SPIONs was compared to loading of aminosilylated S1MPs with carboxylated SPIONs. Silane polymerization (i.e., APTES modification) was carried out for 18 h using a 9% (v/v) APTES solution in isopropyl alcohol (IPA). Loading of the porous silicon matrix was by the incipient wetness method, with retention based on electrostatic interactions. Based on TEM images, the silane polymer blocked nanoparticle access to the pores (Figure 2C). Conversely, the pores of oxidized S1MPs were freely penetrated by SPIONs. High-resolution scanning

NANO MICRO small

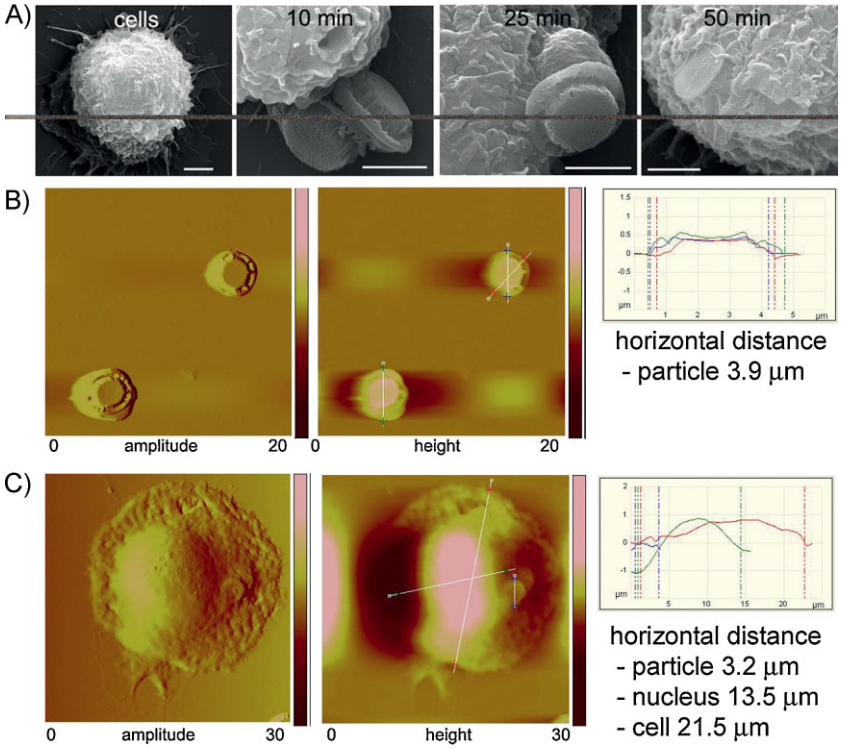

Figure 1. Discoidal S1MP loading with SPIONs. A) SEM images of S1MPs taken at increasing magnification (35k, 60k 150k; bar: 1000, 500, 100 nm). B) TEM images of ultrathin sections of resin-embedded S1MPs taken at increasing magnification (30k, 40k, 100k; bar: 500, 500, 100 nm). C) TEM images of ultrathin sections of S1MPs loaded with SPIONs following surface modification of the S1MPs by either oxidation or oxidation and subsequent APTES (9%) modification (100k; bar: 100 nm). D) High-angle annular dark-field (HAADF)-STEM images showing the porous matrix of an oxidized S1MP loaded with SPIONs (bar: 200 nm (left), 50 nm (right)).

transmission electron microscopy (STEM) images confirmed the presence of SPIONs throughout the porous matrix of the oxidized S1MPs (Figure 2D).

2.3. High-Resolution SEM

To further characterize loading of S1MPs with SPIONs, loaded microparticles were imaged using a high-resolution Hitachi S-5500 SEM instrument (Figure 3A,B). Micrographs, taken at increasing magnification, show 10 nm SPIONs within the porous matrix in close proximity to silicon surfaces (Figure 3A). Larger SPIONs (30 nm) were similarly loaded and were abundant within the porous silicon matrix (Figure 3B).

2.4. MRI of the MDS

MRI of SPION samples was carried out in an actively shielded 7-T Biospec USR70/30 (Bruker Biospin MRI, Billerica, MA) small-animal MRI system equipped with a 30-cm bore, 6-cm gradients (950 mT m^{-1}), and a linear ^{1}H birdcage-style volume resonator with 35 mm inner diameter. S1MPs (5×10^6), control or loaded in the presence of either 10 µg (MDS_{lo}) or 50 µg (MDS_{hi}) of SPIONs (10 nm core), were suspended in phosphate-buffered saline (PBS) alongside pure PBS (blank) in NMR tubes, which were all suspended in water in a specially machined tube holder. The transverse signal relaxation time constant (T_2) of each sample was measured using a Carr–Purcell–Meiboom–Gill echo train (minimum TE = 15 ms, echo spacing 15 ms, 24 echoes, TR = 1100 ms). Effects on the transverse relaxation time (T_2*) due to the susceptibility of SPION were measured using a multigradient echo sequence (minimum TE = 1.5 ms, echo spacing = 3.25 ms, 16 echoes, TR = 4000 ms, 30° excitation). Figure 3C shows axial T_2-weighted fast spin-echo magnetic resonance (MR) images (TE = 65 ms, TR = 5000 ms, ETL = 12, and NEX = 3) of phantoms containing either unloaded S1MPs or MDS. Longer T_2 values for the blank and S1MPs (107 and 88 ms, respectively) result in significantly less negative contrast than for MDS_{lo} ($T_2 = 49$) and MDS_{hi} ($T_2 = 38$ ms) in T_2-weighted spin-echo images. Differences in signal intensity are more dramatic at lower echo times in gradient-echo images, as shown in Figure 3D (TE = 14.5 ms, TR = 4000 ms, 30° excitation). In agreement with T_2 values, T_2* for the blank and S1MP are significantly longer than for the MDS_{lo} and MDS_{hi}.

2.5. Intracellular Trafficking of SPION-Loaded S1MPs (MDS)

To determine the intracellular fate of S1MPs and the MDS, we incubated J774A.1 macrophages with ten MDSs per cell for 24 h at 37 °C. Five internalized S1MPs, in different orientations, are shown in Figure 4A. Higher-magnification images of the three boxed S1MPs are shown to the right. A cell with two MDSs is shown in Figure 4B, with higher-magnification images of the MDSs shown to the right. Clusters of S1MP-released 10 nm SPIONs (black arrows) are indicated in the high-magnification images. Vesicular membranes surrounding unloaded S1MPs are tightly associated with the microparticles (S1MPs). In contrast, membranes surrounding MDSs appear to "relax" or expand in the presence of the released SPIONs. The intracellular fate of the S1MP-released SPIONs and the impact of nanoparticle surface coating are under investigation.

2.6. Characterization of APTES Polymerization on Porous Silicon

AFM was used to compare the roughness and surface height of an oxidized porous silicon wafer (Figure 5A) with that of an APTES-modified wafer (Figure 5B). Piranha-oxidized porous silicon wafers were incubated with 0.5% APTES (v/v) for 4 h at room temperature. Silane polymerization increased the height of the surface features from 0.689 to 3.843 nm.

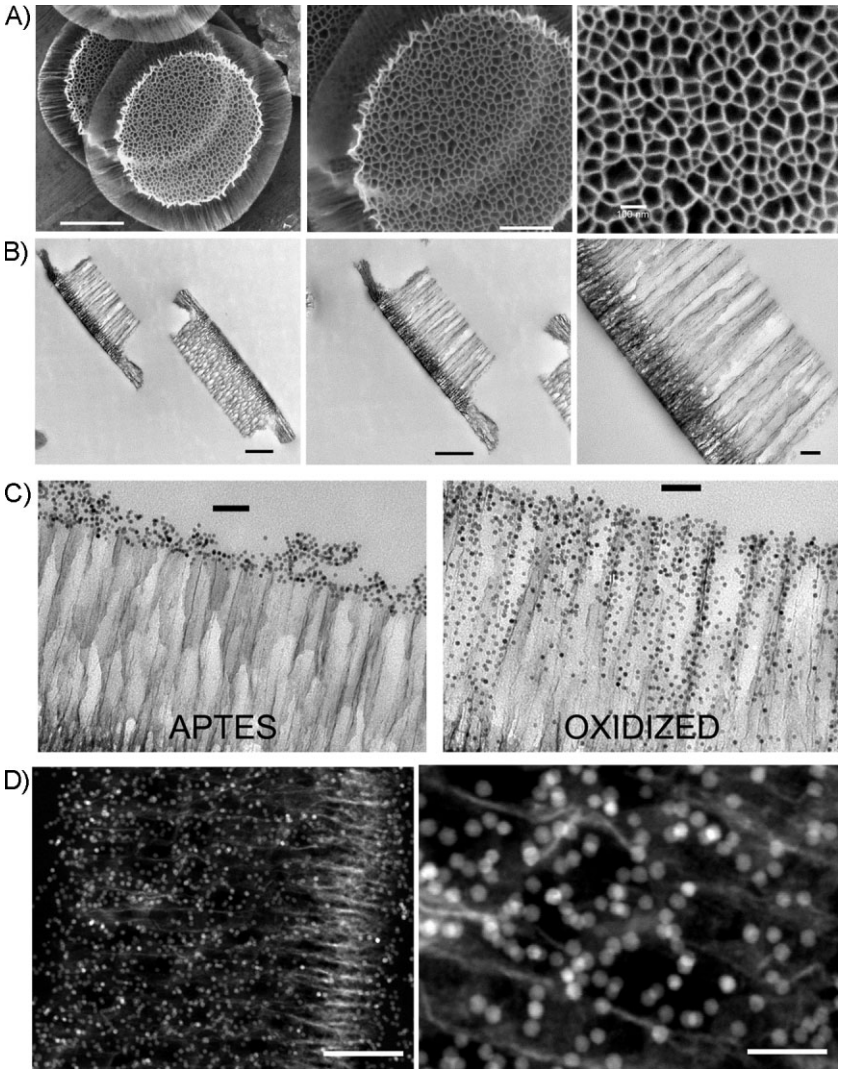

Figure 2. Cellular engulfment of S1MPs by J774A.1 macrophages. A) SEM images of J444A.1 cells incubated with S1MPs (at a ratio of 1:5) for different lengths of time, which demonstrate particle orientation during uptake and varying degrees of internalization (10k, 50k, 50k, 40k; bars: 2 μm). B) AFM amplitude and height images, including section analysis, which demonstrate the height and diameter of S1MPs. C) AFM image and section analysis of a J774A.1 cell following internalization of S1MPs (1:5 ratio).

Elemental analysis of silane-modified surfaces by X-ray photoelectron spectroscopy (XPS) demonstrated similar amounts of nitrogen on aminosilylated surfaces at 2 h, regardless of the concentration of APTES present in solution (Figure 5C–E). After 4 h of incubation, the atomic percent of nitrogen was significantly greater in the 9% APTES sample than in the 2% ($p < 0.02$) sample. A similarly significant increase in atomic percent of nitrogen was present in the 9% APTES sample after 22 h, compared to both the 0.5% ($p < 0.0004$) and the 2% ($p < 0.009$) samples. The increase in incubation time from 2 to 4 h did not significantly increase the atomic percent of nitrogen on the silicon surface, but extended incubation at 22 h significantly increased the atomic percent of nitrogen for the 0.5% ($p < 0.02$) and 9% ($p < 0.002$) APTES samples. The increase in atomic percent of nitrogen directly corresponds to an increase in polymer thickness. Surface roughness, caused by an inhomogeneous layer across the surface, was also positively correlated with incubation time, as shown in Figure 5F. The roughness of the silicon surface increased significantly with each increase in incubation time (0 versus 2 h, $p < 0.0005$; 2 versus 4 h, $p < 0.0001$; 4 versus 22 h, $p < 0.002$). The combined increase in surface height, atomic percent of nitrogen, and surface roughness with time and APTES concentration is consistent with the presence of an extensive polymer coating surrounding the porous silicon matrix after 22 h of incubation in 9% APTES (v/v).

2.7. Quantification of SPION Load in S1MPs

S1MPs were loaded with increasing concentrations of SPIONs, and a nonlinear fit of the data was performed using Graph Pad Prism ($R^2 = 0.8029$; Figure 6A). SPION loading and retention within S1MPs increased linearly with concentrations ranging from 0.01 to 5 mg mL^{-1} iron (borate buffer, pH 5.0), after which a plateau was reached. The amount bound represents the amount of iron present in 3×10^6 S1MPs. Loading efficiency, based on loading 1×10^7 S1MPs in the presence of 1 mg mL^{-1} of iron (10 μg; 10 nm SPIONs) was 19%; however, this was based on Prussian blue analysis of unbound and bound SPIONs, which only accounted for 20% of the original iron.

Having previously observed capping of the porous silicon matrix by a multilayer silane polymer during the loading process, the ability of the silane polymer to trap SPIONs within the porous matrix of oxidized S1MPs was evaluated (Figure 6B). S1MPs were loaded with SPIONs and retention within the pores by electrostatic forces was compared to retention of SPIONs following APTES polymerization for varying lengths of time using a 9% (v/v) APTES solution. Association of SPIONs with S1MPs was more than double (224%) following overnight incubation with APTES, perhaps due to both enhanced retention and entrapment of SPIONs in the dense silane polymer. The zeta potential of all particle formulations, measured in 4 mM sodium acetate (pH 6.5), is displayed in Table 1.

2.8. STEM/Energy-Dispersive X-ray Spectroscopy

To confirm the presence of SPIONs in the porous silicon matrix following loading and capping, S1MPs were loaded with SPIONs, then sectioned with a microtome into ultrathin slices (70 nm) and analyzed by high-angle annular dark-field (HAADF)-STEM combined with elemental maps from

NANO MICRO small

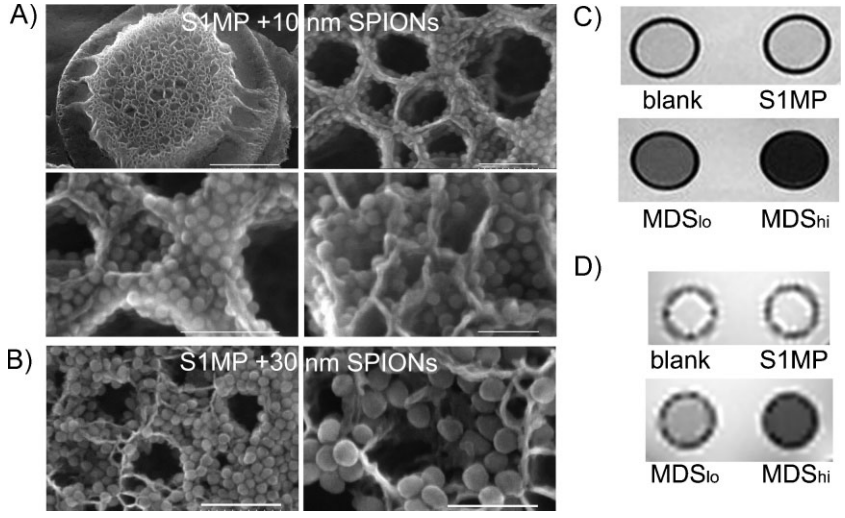

Figure 3. High-resolution SEM and MRI. S1MPs loaded with SPIONs at increasing magnifications. A) S1MP loaded with 10 nm SPIONs (25k, 300k, 500k, 600k; bar: 1 μm, 100 nm, 100 nm, 50 nm). B) S1MP loaded with 30 nm SPIONs (200k, 450k; bar: 200, 100 nm). C,D) Axial spin- (C) and gradient- (D) echo MR images of NMR tubes containing PBS (blank), S1MPs, and MDS loaded with low (MDS_{lo}) or high (MDS_{hi}) levels of SPIONs.

energy-dispersive X-ray spectroscopy (EDX) using an FEI Tecnai G2 F20 X-Twin TEM instrument at an accelerating voltage of 200 kV (Figure 6C). EDX elemental analysis was performed on the boxed region of the loaded S1MP. The presence of silicon (Si-K) and oxygen (O-K) was verified and the iron signal (Fe-K and Fe-L) was found to co-localize with SPIONs in the STEM image. The spectrum in Figure 6D is a representative elemental analysis of the boxed region.

2.9. S1MP Degradation and Release of SPIONs

SPION-loaded S1MPs (MDS), in the presence and absence of an APTES cap, were incubated on a rotator at 25 °C for 23 h in PBS and dissolution of the silicon particles was determined at various time points by inductively coupled plasma–optical emission spectroscopy (ICP-OES) analysis of the supernatant (Figure 6D). No degradation was detected at 1 and 2 h. After 4 h, silicon particles, capped and not capped, were 94 and 87% intact, respectively, but this decreased to 83 and 80% at 8 h, and 46% for both groups at 23 h. These data support greater than 50% degradation of the silicon particles at 23 h in the presence of PBS at room temperature. Aminosilylation of the loaded S1MP did not alter the rate of degradation. In a separate experiment using quasi-hemispherical S1MPs, degradation of SPION-loaded S1MPs and release of iron were monitored by measuring the iron and silicon content in filtered (0.45 μm) supernatant following incubation of the MDS in fetal bovine serum (FBS) at 37 °C, with sample rotation (Supporting Information, Figure 1). Under these conditions, silicon degradation was more rapid, with 31% S1MP degradation at 4 h and 96% degradation at 24 h. SPION release paralleled S1MP degradation at most time points, with the exception of greater release (54%) compared to degradation (31%) at 4 h. Degradation of porous silicon particles is very rapid in PBS and serum, with both release of SPIONs and degradation being greater than 50% at 24 h under all conditions tested. However, in the presence of diverse biophysical conditions, such as cellular uptake and acidic endosomal encapsulation, in vivo particle degradation is much slower (see Section 2.11).

2.10. MTT Proliferation Assay

The viability of J774A.1 cells in the presence of each particle presentation was measured using a 3-(4,5-dimethylthiazol-2-yl)-2,5-diphenyltetrazolium bromide (MTT) proliferation assay at 24–96 h (Figure 6E). No significant differences in cell growth were measured for any group across all time points.

2.11. In vivo Stability of the MDS

The impact of capping the MDS through aminosilylation on the in vivo stability of the assembled construct was tested by injecting mice (tail-vein) with either control, unloaded S1MPs or S1MPs loaded with SPIONs in the absence and presence of the silane cap. Tissues were harvested at 2 and 24 h after particle introduction and sections from the lungs, liver, and spleen were stained with Prussian blue and Nuclear Fast Red to visualize the SPIONs. In all spleen samples, iron was loosely associated with S1MPs (Figure 6F). In the liver and lungs, uncapped and capped MDSs displayed overlap of S1MPs and iron staining at 2 h, which indicated that the MDS was intact. After 24 h, S1MPs were intact and association with SPIONs was evident; however, in the absence of the silane cap, SPIONs appeared to be migrating away from the uncapped S1MPs. These data support enhanced retention of SPIONs in first-stage porous silicon particles following silane capping. Control, unloaded S1MPs were negative for iron staining (not shown).

2.12. In vitro Targeting of the MDS with Endothelial-Specific Antibodies

To enhance cell-specific association of the MDS with vascular endothelial cells, either anti-VEGFR-2 or PECAM antibody was covalently conjugated to the MDS surface following nanoparticle loading and APTES capping. Figure 7A–C shows confocal images of immunoglobulin G (IgG) isotype control (Figure 7A) and anti-VEGFR-2 (Figure 7B,C) antibody-labeled MDSs and their association with human umbilical vein endothelial cells (HUVECs). While the control IgG-labeled MDSs were predominantly independent of the cells, anti-VEGFR-2 antibody-labeled MDSs were found in association with endothelial cells. To determine if the targeted MDS particles were internalized by HUVECs, a z-stack of a magnified cell is shown in Figure 7C (center image). The actin cytoskeleton, stained with rhodamine phalloidan, lies beneath the MDS, thus indicating surface attachment. The far-right image in Figure 7C shows two adjacent endothelial cells with MDS units located among extended lamellopodia. Fluorescein-

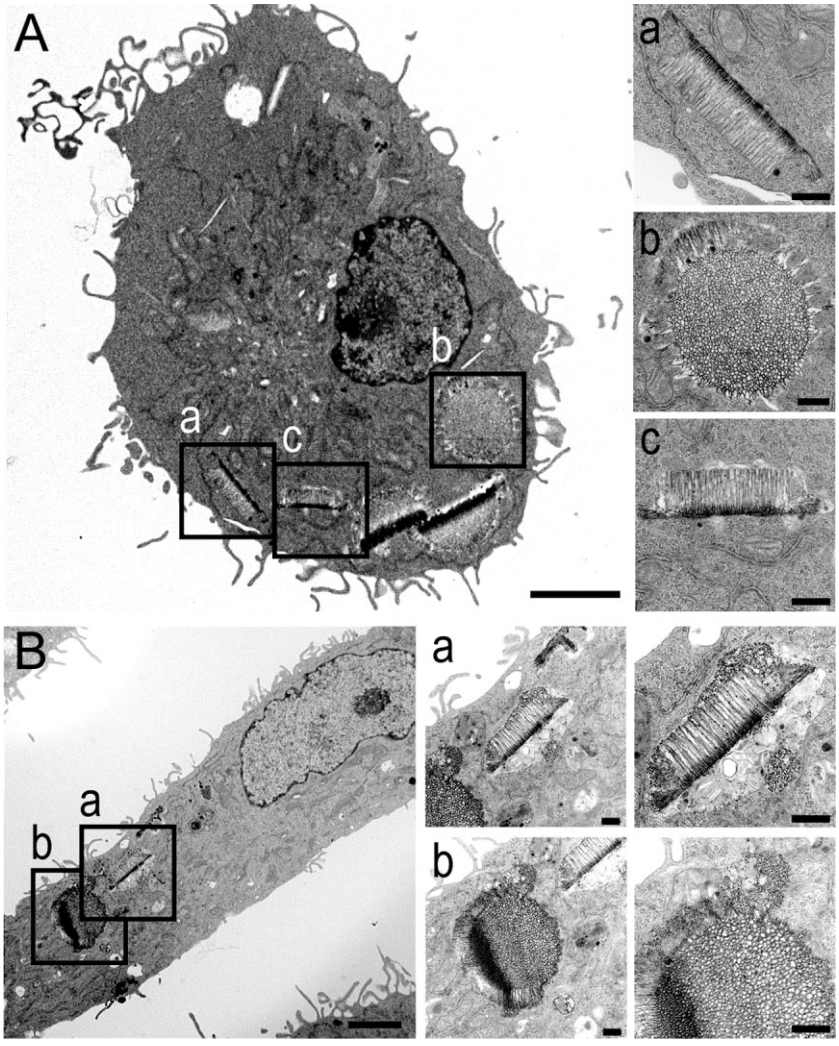

Figure 4. Intracellular trafficking of the MDS. TEM images of ultrathin sections of J774A.1 cells 24 h after introduction of either control (A) or SPION-loaded (B) S1MPs (at a ratio of 1:5). Cells are shown to the left at 6k magnification (bar: 3 μm) and to the right at 25k and 50k magnification (bars: 500 nm). Internalized S1MPs can be seen in different orientations, with clusters of SPIONs indicated by black arrows.

conjugated antibodies were used in the study for imaging and to quantify bound antibody by flow cytometric analysis. The number of antibody molecules bound per MDS was calculated based on a standard curve created using Quantum Simply Cellular antimouse IgG beads. Analysis of isotype control or anti-VEGFR-2 antibody-labeled particles indicated that each particle had approximately 17 000 antibody molecules on its surface (Figure 7D).

Endothelial-specific association of the targeted MDSs was quantitated across two endothelial cell lines, HUVECs and human microvascular endothelial cells (HMVECs), using control IgG and anti-PECAM antibody-labeled MDSs. Binding was quantified by measuring the percentage of cells with high side scatter (minus side scatter from control cells). HUVECs and HMVECs associated significantly more with anti-PECAM-labeled MDSs than control IgG-labeled MDSs, and displayed an 8.8-fold ($p < 0.03$) and 1.7-fold ($p < 0.004$), respectively, enhancement in binding in the presence of endothelial-specific antibody.

3. Discussion

In this study, the assembly of a multi-particle MDS with targeting and potential imaging capabilities was demonstrated. The first-stage porous silicon carriers, S1MPs, are biodegradable and biofunctional due to porosification and oxidation, respectively. The S1MPs are mathematically designed to possess geometric properties that both enhance vascular migration and manipulate cellular uptake.[24] Herein, we show that S1MPs are internalized by J774A.1 mouse macrophages. SEM images demonstrate multiple stages of S1MP uptake over time. Internalization of S1MPs was further supported by AFM images that indicated the presence of S1MPs beneath the cell surface. As reported by others, phagocytic blood monocytes/macrophages migrate to sites of inflammation,[25] and have been reported to serve as carriers for particles to inflamed and necrotic regions,[26,27] such as those found in tumor tissue. Thus, cellular uptake of delivery vectors by monocytes/macrophages may provide a means for delivering non-targeted MDSs to cancer lesions.

Overnight incubation of oxidized S1MPs with 9% (v/v) APTES created a multilayer silane polymer that interfered with SPION loading. However, the hydrophilic, negatively charged surface of oxidized S1MPs permitted association with SPIONs. Following loading, high-resolution STEM and SEM images show large numbers of SPIONs throughout the porous matrix. SPIONs adhere to the silicon surface, simultaneously coating the pores and concentrating the SPIONs within the S1MPs. Delivery of a single MDS to a cell would constitute delivery of a multitude of nanoparticles, which should enhance both cell tracking and therapeutic efficacy for drug-loaded nanoparticles. Phantom models containing the MDS had shortened T_2 and T_2* relaxation times in a manner dependent on SPION concentration. MDS_{lo} MRI phantoms contained 5×10^6 MDSs in 600 μL of PBS (14 fM iron based on 100% loading efficiency). The mice in this study were injected with 1×10^8 MDS in 100 μL of PBS, which corresponded to a dose 120 times more concentrated than the MRI phantom, with 20 times the dose of particles. The in vivo detection threshold for SPIONs is reported to be femtomole quantities, with several studies reporting MRI detection of a few hundred SPION-labeled cells.[28]

TEM images of noncapped, loaded MDSs following internalization by macrophages show SPIONs being released from S1MPs 24 h after internalization. The SPIONs are

small NANO MICRO

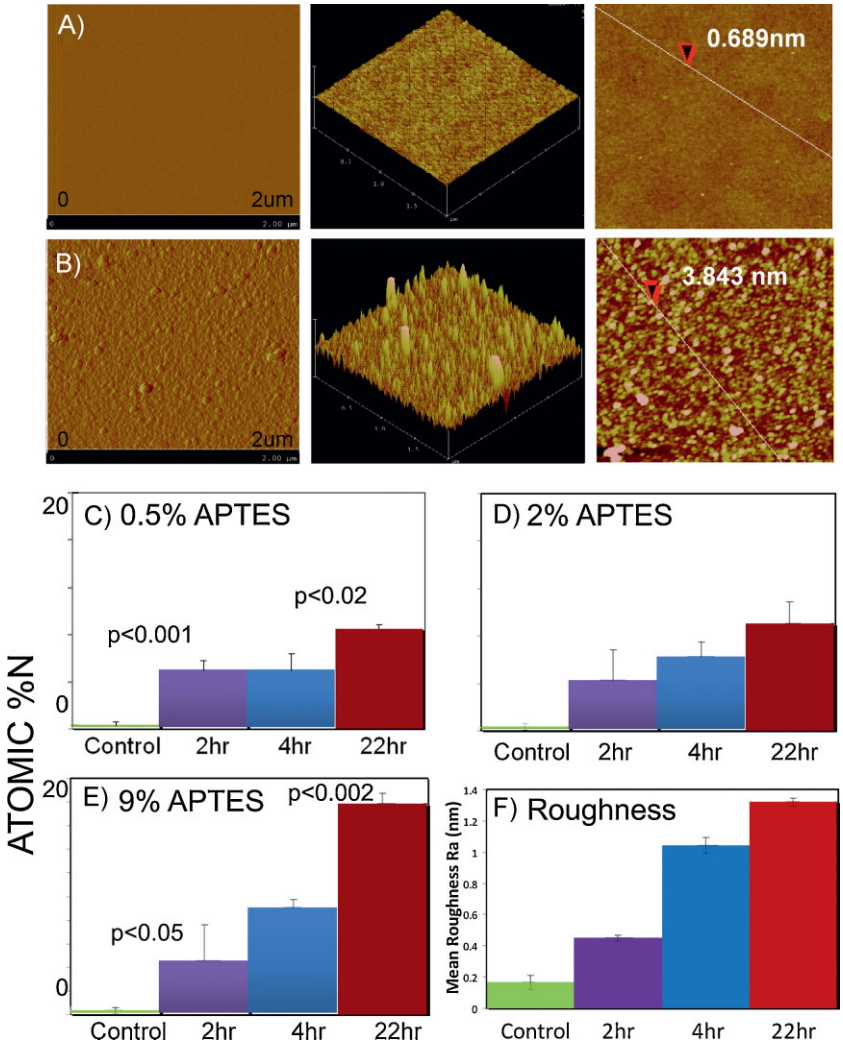

Figure 5. Surface height and roughness of chemically modified porous silicon. A,B) AFM images of amplitude, three-dimensional (3D) structure, and height of oxidized (A) and APTES-modified (B) (0.5% for 4 h) porous silicon. C–E) XPS analysis of atomic % nitrogen on the porous silicon surface determined at various time points for APTES polymerization using 0.5 (C), 2 (D), and 9% (E) solutions (v/v) of APTES. F) Surface roughness is presented at each time point for porous silicon modified with 0.5% APTES.

clustered and appear to be actively sorted to specific regions of the vesicles. The appearance of multiple vesicular bodies within the phagosomal units, and the possible sorting of its contents, is indicative of activities found in sorting endosomes.[29] The final subcellular destination and the impact of second-stage nanoparticle (i.e., SPION) surface coating and size on intracellular trafficking are under investigation.

Blockade of loading the porous silicon matrix with SPIONs by aminosilylation led us to study the impact of silane concentration and reaction time on the resulting silane polymer. Modification of the oxidized porous silicon surface with APTES at both increasing concentration and incubation time positively correlated with an increase in surface height, atomic percent of nitrogen, and surface roughness of the silicon surface, as previously reported by others.[30] Multiple layers of crosslinked silane molecules contribute to the increased surface height.[31] Based on the extensive coating (i.e., capping) of the porous silicon matrix following overnight incubation with APTES, oxidized S1MPs were first loaded with SPIONs and then capped by aminosilylation of the particle surface. Aminosilylation of the loaded S1MPs for 2–4 h did not alter the amount of loaded SPIONs; however, extension of the reaction time to 16 h more than doubled the amount of SPIONS associated with S1MPs. It is believed that the extensive polymer coating may both prolong retention of SPIONs within the porous matrix and induce capture of additional SPIONs within the multilayer polymer coat. Confirmation of loading and retention of SPIONs within the S1MP pores during the APTES capping procedure comes from HAADF-STEM images and EDX elemental mapping of particles within the pores.

Cellular compatibility of the loaded and capped particles was supported by in vitro proliferation assays, which demonstrated similar macrophage proliferation following incubation with all particle formulations. Previously we reported a similar lack of cytotoxicity for endothelial cells incubated with SPION or gold nanoparticle-conjugated S1MPs.[32] Enhanced in vivo retention of SPIONs in capped MDSs was supported by intravascular injection of the MDSs into mice and subsequent co-localization of S1MPs and iron by histological analysis of lung, liver, and spleen. These tissues were selected based on earlier findings by our group, which showed preferential localization of nontargeted discoidal silicon microparticles in the tissues.[33]

In vitro degradation studies indicated that 54% of the silicon content from SPION-loaded S1MPs is released into solution after incubation in PBS for 23 h at 25 °C with motion. The presence of surface aminosilylation on loaded S1MPs did not impact the degradation rate. Conversely, TEM images of macrophages with internalized MDSs at 24 h did not support high levels of S1MP degradation, perhaps due to confinement of the particles within acidic vesicular compartments. Rapid cell-free degradation of S1MPs at 37 °C in FBS and the parallel release of SPIONs supports a release mechanism that is driven predominantly by the rate of S1MP degradation under cell-free conditions; however, intracellular release and trafficking of SPIONs is more complex and is currently under investigation.

In addition to particle "capping", aminosilylation of loaded S1MPs provided substrates for attachment of endothelial-specific antibody. Preliminary in vitro studies supported enhanced endothelial association with anti-VEGFR-2 and anti-PECAM antibody-conjugated MDSs, compared to

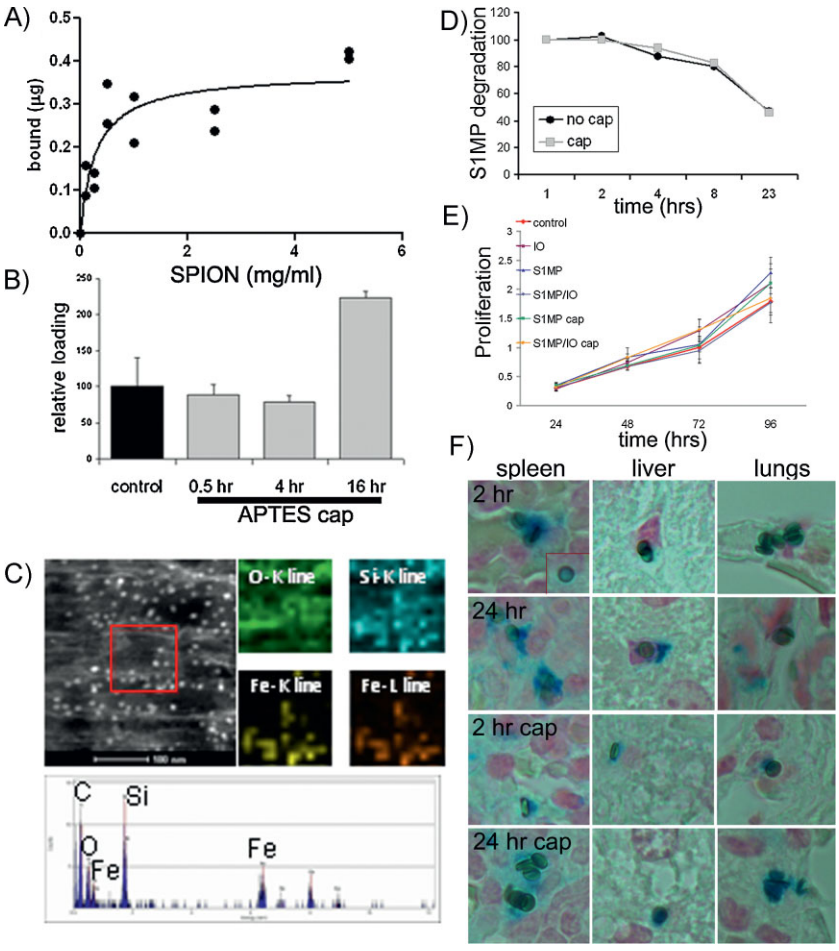

Figure 6. Loading and retention of SPIONs in S1MPs. A) Loading curve for S1MPs loaded with SPIONs. Iron load was based on Prussian blue analysis of the loaded S1MPs. B) Effect of APTES "capping" on loading with SPIONs. C) EDX elemental mapping confirming the presence of SPIONs in the porous silicon matrix following capping with APTES (left: the red box indicates the area of the HAADF-STEM image analyzed by EDX). Intensity maps for relevant elements present in the sample are presented. Bottom row: typical EDX spectrum. D) Degradation of SPION-loaded S1MPs in PBS at 37 °C with time. E) MTT proliferation assay of J774A.1 cells incubated with SPIONs (IO), S1MPs (oxidized or APTES-capped), or MDS (S1MP/IO). F) Prussian blue staining of lung, spleen, and liver harvested from mice at 2 and 24 h after injection of 1×10^8 MDSs, capped or uncapped (bar: 10 μm).

isotype control IgG-labeled MDSs, in the presence of serum across two endothelial subtypes, HUVECs and HMVECs.

4. Conclusions

This study demonstrates the assembly of a targeted, multistage (multiparticle) delivery system with potential as a contrast agent for MRI by entrapment of SPIONs in a porous silicon matrix.

5. Experimental Section

Porous silicon microparticle fabrication: Porous silicon particles were fabricated in the Microelectronics Research Center at The University of Texas at Austin. Silicon particles, featuring a mean diameter of 3.2 ± 0.2 μm and an average pore size of 51.3 nm, were fabricated by modification of protocols recently published by our laboratory.[6] Briefly, heavily doped p++-type (100) silicon wafers with a resistivity of 0.005 Ω cm (Silicon Quest, Inc., Santa Clara, CA, USA) were used as the silicon source. A 40 nm SiO_2 layer was thermally grown on the wafer at 950 °C, followed by an 80 nm layer of silicon nitride (SiN) deposited by low-pressure chemical vapor deposition. Standard photolithography was used to pattern a 2 μm circular pattern with 2 μm pitch over the wafer using a contact aligner (K.Suss MA6 mask aligner) and PR-1000A photoresist (Futurrex Franklin, NJ, USA). The pattern was transferred into the SiN by dry etch in CF_4 plasma (Plasmatherm 790, 25 sccm CF_4, 100 mTorr, 200 W RF, 2 min), and into the SiO_2 by wet etch in 5% HF for 1.5 min to prevent overetching into the silicon. Silicon particles with both mechanical stability and high porosity were then formed by a three-step electrochemical etch in HF/ethanol (1:3) solution. An initial low-porosity layer of thickness approximately 20 nm was formed by applying a 10 mA cm^{-2} current for 10 s. The electrical current was then smoothly increased to 100 mA cm^{-2} over the course of 15 s forming a 70-nm-thick layer of transition between low porosity and high porosity, and the 100 mA cm^{-2} current was applied for 30 min forming a 600 nm porous layer. Finally a 380 mA cm^{-2} current was applied for 6 s forming a release layer. The masking SiN and SiO_2 layers were removed in 49% HF, and the silicon particles released from the substrate by sonication in isopropanol. Quasi-hemispherical S1MPs had a mean particle diameter of 3.2 ± 0.2 μm, with an average pore size of 26.3 nm. Processing details were recently published by our group.[6]

Table 1. Zeta potential (mV) for each population of particles.

	NH_2 SPION	Oxid. S1MP	APTES S1MP	Oxid. S1MP +NH_2 SPION	Capped MDS
Surface charge	−5.89	−16.22	35.61	−5.79	26.16

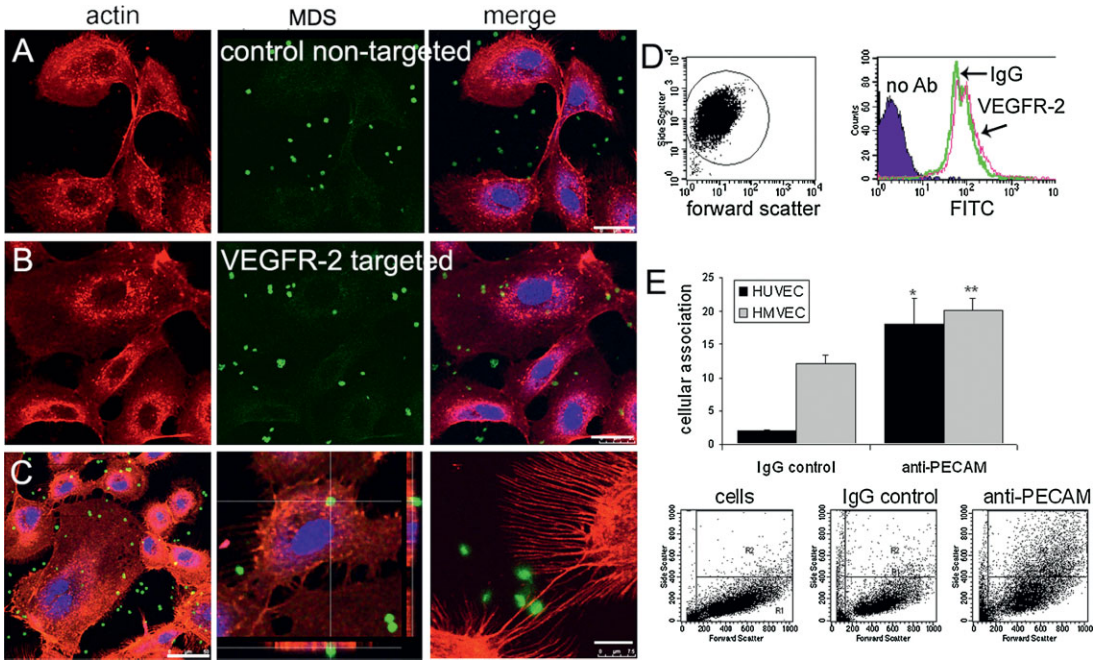

Figure 7. Endothelial targeting with the assembled MDSs. A) HUVECs were incubated with either control IgG fluorescein-labeled MDSs (A) or anti-VEGFR-2 fluorescein antibody-labeled MDSs (B,C) for 2 h at 37 °C (10:1 ratio of particles to cells). C) Antibody-targeted cells are shown at two magnifications, with 3D images at the crosshairs of the higher magnification image (middle). To the right, lamellopodia projecting from two cells make contact with the MDS (63× oil immersion lens; A,B) bar 25 μm, C) bars 50 and 7.5 μm; actin: rhodamine phalloidin; nuclei: DRAQ5). D) Flow cytometry dot plot (left) showing microparticle light scatter and a histogram (right) showing microparticle fluorescence before and after conjugation with fluorescent antibody. E) Bar graph (top) showing the relative association of the MDSs with HUVEC and HMVEC endothelial cells conjugated with either control IgG or anti-PECAM-specific antibody. Below are representative flow cytometry dot plots showing the increase in side scatter in HUVECs after incubation with targeted (anti-PECAM) MDSs.

Surface modification of porous silicon microparticles: The IPA suspension containing S1MPs was transferred to a glass beaker and the IPA was evaporated overnight using a hotplate set at 110 °C. The dried S1MPs were then treated with piranha solution (1 volume H_2O_2 and 2 volumes H_2SO_4) with heating to 110–120 °C for 2 h with intermittent sonication to disperse the S1MPs. The suspension was then washed in deionized (DI) water until the pH of the suspension was higher than 5.5.

Oxidized S1MPs were washed in IPA three or four times, and then suspended in IPA containing 0.5–9% (v/v) APTES (Sigma–Aldrich, St. Louis, MO) for 0.5–22 h at 35 °C and 1300 rpm. The APTES-modified S1MPs were washed in IPA and the surface charge was evaluated by zeta potential analysis.

AFM: J774A.1 cells, grown on collagen-coated glass coverslips, were treated with S1MPs in Dubelcco's modified Eagle's medium (DMEM) containing 10% fetal calf serum (FCS) and antibiotics for 60 min at 37 °C at a cell-to-particle ratio of 1:5. Cells were fixed in 4% formaldehyde overnight at 4 °C, washed with nanopure water, and allowed to dry in a sterilGARD III flow hood prior to imaging. AFM was conducted using a Veeco di BioScope II instrument integrated with a Nikon TE2000 inverted optical microscope. Scanning was performed using the tapping mode in air and rotated tapping-mode etched silicon probe (RTESP) cantilevers (fo = 262–325 kHz, k = 20–80 N m^{-1}). Image analysis was performed with the Research NanoScope software version 7.30.

For AFM imaging of oxidized versus APTES-modified porous silicon, continuous porous layers were formed on silicon wafers by electrochemical etching using the same parameters described for silicon microparticles. The surface of the wafer was evaluated for height and roughness using a Veeco Nanoscope III (Digital Instruments) apparatus in tapping mode in air and TESP cantilevers (fo = 320 kHz, k = 42 N m^{-1}).

XPS: Elemental analysis and evaluation of chemical bonding on the modified silicon wafers were performed using a PHI Quantera X-ray photoelectron spectrometer equipped with a monochromatic Al Kα radiation source (1486.6 eV) with a power setting of 350 W and analyzer pass energy of 69.0 eV.

Loading S1MPs: Aliquots containing 3–5 × 10^6 oxidized (negative) or APTES (9% (v/v), 22 h)-modified (positive) S1MPs were dried overnight either by thermal heating at 37 °C or at room temperature in a vacuum desiccator. Favorably charged SPIONs (amine- or carboxy-modified, respectively; Fe_3O_4/Fe_2O_3; 10–15 or 30 nm; purchased from Ocean NanoTech, LLC, Springdale, AR) were added to the dry S1MPs at concentrations ranging from 0.1 to 5 mg mL^{-1} in a total volume of 10–25 μL. Borate buffer was used for loading by the incipient wetness method[34–36] (0.01 M, pH 5.0 for amine-modified SPIONs, and 50 mM, pH 8.5 for carboxylic acid-modified SPIONs). For loading, particles were briefly sonicated, then incubated at room temperature with agitation (1300 rpm) for 10 min followed by no motion for 20 min. Samples were then centrifuged at 4200 rpm (Beckman Coulter Allegra X-22 centrifuge equipped with a 296/06 rotor) for 5–10 min and the pellet was washed with water (50 μL) to remove free iron oxide. For STEM and TEM imaging, the loaded S1MPs

were suspended in 2% agarose, cut into 1-mm slices, and suspended in water. Samples were then dehydrated with a series of increasing ethanol concentrations (50, 70, 95, 100%) with the final dehydration step at 100% repeated twice (20 min per step), followed by two washes in 100% acetone. The samples were then infiltrated with Spurr's resin at resin/acetone concentrations of 1:2, 2:1, and 1:0 for 2–4 h for each condition. The samples were then embedded in fresh Spurr's resin, with polymerization performed at 70 °C for 8 h. For high-resolution SEM imaging of the loaded S1MPs, washed samples were resuspended in water (50 μL) and an aliquot was dried on an SEM specimen stub. Samples were imaged using a Hitachi S-5500 microscope at 30 kv.

Entrapment and quantification of SPIONs: For APTES capping of the porous silicon matrix post-loading, oxidized S1MPs (5×10^6) were loaded with SPIONs (25 μg; amine modified) in borate buffer (25 μL), then centrifuged and washed twice in fresh borate buffer. Loaded S1MPs were then resuspended in a 9% (v/v) APTES solution in IPA (50 μL) for 0.5, 4, or 16 h in a thermomixer at 23 °C at 1300 rpm. The particles were then washed twice in IPA and resuspended in a final volume of 50 μL. Iron oxide loading and entrapment (i.e., "capping") were quantitated using a Prussian blue iron assay.[14] An aliquot from each sample (5 μL) was heated at 50 °C in 6N HCl (120 μL) for 2 h with agitation to convert SPIONs into free iron. Iron was then oxidized using ammonium persulfate (0.1 mg mL^{-1}; BioRad, Richmond, CA) and the color reaction was initiated by adding 5% $K_4[Fe(CN)_6] \cdot 3H_2O$ (125 μL; Sigma–Aldrich) for 10 min. A standard curve was generated using iron(III) hexahydrate (Sigma–Aldrich), and the absorbance was read at 690 nm using a Molecular Devices M5 plate reader spectrophotometer.

MRI phantoms: MR phantoms were prepared in 5-mm thin-walled NMR tubes (Wilmad Labglass, Vineland, NJ) using S1MPs (5×10^6) loaded with 10 nm SPIONs (10 or 50 μL, 1 mg mL^{-1}) suspended in PBS (600 μL). Sample sets of four or five phantoms, including a PBS-only control, were moved into a specially machined tube holder which was placed into a 50-mL centrifuge tube. The tube was then filled with water to reduce interference from air interfaces, doped with 0.1% Magnevist (v/v), capped, and imaged. The characteristic transverse relaxation times, T_2 and T_2*, were measured using spin-echo and multiple gradient-echo sequences as specified in the Results section.

STEM/EDX spectroscopy: S1MPs loaded with SPIONs were cut into ultrathin sections using a microtome (Leica, Deerfield, IL) and analyzed by HAADF-STEM combined with elemental maps from EDX spectroscopy using a FEI Tecnai G2 F20 X-Twin TEM instrument at an accelerating voltage of 200 kV, set at nanoprobe spot mode #7, and tilted at an angle of 12°. The EDX spectrum was sampled in 225 spots on a 15×15 grid (see box in Figure 6D), with a dwell time of 8000 ms per spot.

SEM: For particle imaging, S1MPs suspended in either IPA or water were dried on ethanol-washed SEM stubs (Ted Pella, Inc., Redding, CA) overnight in a desiccator. For cell-based imaging, J774A.1 murine macrophage cells, purchased from American Type Culture Collection (Manassas, VA), were cultured in DMEM containing 10% FBS, streptomycin (100 μg mL^{-1}), and penicillin (100 U mL^{-1}) (Invitrogen; Carlsbad, CA). J774A.1 cells were plated in a 24-well plate containing 5×7 mm^2 silicon chip specimen supports (Ted Pella, Inc.) at 7.5×10^4 cells per well. After 22 h, medium containing S1MPs (1:5 cell/microparticles, 0.5 mL well^{-1}) was introduced and the cells were incubated at 37 °C for 10, 25, or 50 min. Samples were fixed in 2.5% glutaraldehyde for 30 min (Sigma–Aldrich; St. Louis, MO), then dehydrated in increasing concentrations of ethanol, followed by incubation in a 50% alcohol–hexamethyldisilazane (HMDS; Sigma) solution for 10 min, with a final incubation in pure HMDS for 5 min to prepare for overnight drying in a desiccator. Specimens were mounted on SEM stubs (Ted Pella, Inc.) using conductive adhesive tape (12 mm OD PELCO Tabs, Ted Pella, Inc.). Samples were sputter-coated with a 10 nm layer of gold using a Plasma Sciences CrC-150 sputtering system (Torr International, Inc.). SEM images were acquired under high vacuum, at 20.00 kV and spot size 5.0, using a FEI Quanta 400 FEG ESEM apparatus equipped with an ETD (SE) detector. High-resolution images were acquired using a Hitachi S-5500 In-lens FE-SEM.

TEM: J774A.1 cells were plated at 2×10^5 cells per well in a six-well cell culture plate. After 22 h, S1MPs, both loaded and control unloaded, were introduced at a cell/microparticle ratio of 1:5 at 37 °C for 24 h. The cells were then washed and fixed in a solution of 2% paraformaldehyde (Electron Microscopy Sciences; Hatfield, PA) and 3% glutaraldehyde (Sigma–Aldrich) in PBS, pH 7.4, for 1 h at room temperature. After fixation, the samples were washed and treated with 0.1% cacodylate-buffered tannic acid, post-fixed with 1% buffered osmium tetroxide for 30 min, and stained with 1% uranyl acetate. The samples were dehydrated in increasing concentrations of ethanol, infiltrated, and embedded in Poly-Bed 812 medium. The samples were polymerized in an oven at 60 °C for 2 days. For both cell and S1MP samples, ultrathin sections were cut in a Leica Ultracut microtome (Leica, Deerfield, IL), stained with uranyl acetate and lead citrate in a Leica EM Stainer, and examined in a JEM 1010 transmission electron microscope (JEOL, USA, Inc., Peabody, MA) at an accelerating voltage of 80 kV. Digital images were obtained using the AMT Imaging System (Advanced Microscopy Techniques, Danvers, MA).

Antibody conjugation: Anti-PECAM antibody was obtained from Sigma, while anti-VEGF R2/KDR (vascular endothelial growth factor receptor) and isotype control (IgG_1) fluorescein-conjugated antibodies were purchased from R&D Systems (Minneapolis, MN). Antibodies were covalently attached to APTES-capped/loaded S1MPs (i.e., MDS) according to the Pierce Biotechnology (Thermo Scientific Inc., Rockford, IL) manufacturer's protocol entitled "EDC/NHS Crosslinking of Carboxylates and Primary Amines". For conjugation, each reaction contained 5×10^6 S1MPs and 10 μg antibody in a final volume of 250 μL.

Flow cytometry: HMVECs, a kind gift from Rong Shao at Baystate Medical Center/University of Massachusetts, were cultured in Clonetics EGM Endothelial Cell Growth Medium (Lonza; Walkersville, MD), while HUVECs were purchased from Lonza Walkersville, Inc., and maintained in EBM-2 medium (Clonetics). HUVECs or HMVECs (1.5×10^5 cells well^{-1}) were seeded into six-well plates and 24 h later the cells were incubated with the 4×10^6 silicon microparticles per well in complete media for 60 min. Microparticle association with cells was determined by measuring the increase in side scatter using a Becton Dickinson FACSCalibur flow cytometer equipped with a 488-nm argon laser and CellQuest software (Becton Dickinson; San Jose, CA). Quantitation of antibody conjugated to the MDS was determined using a Becton Dickinson FACSCalibur flow cytometer equipped

with a 488-nm argon laser and CellQuest software (Becton Dickinson; San Jose, CA). Antigen density calculations were based on a QuickCal calibration curve generated with Quantum Simply Cellular antimouse IgG (Bangs Laboratories, Inc.; Fishers, IN).

Confocal microscopy: HUVECs were grown on No.1.5 glass coverslips. When 80% confluent, the cells were incubated with loaded and capped antibody-conjugated S1MPs (1:10, cell/S1MP) for 120 min in complete media at 37 °C. Cells were then washed with PBS, fixed with 4% formaldehyde, and permeabilized with 0.1% Triton X-100. PBS containing 1% bovine serum albumin (BSA) was used as a blocking agent prior to incubation with 200 nM rhodamine-conjugated phalloidin (Invitrogen; Carlsbad, CA) and DRAQ5 (2 μL mL^{-1}; Biostatus Limited, UK) for 20 min. The coverslips were then washed and mounted on glass slides using Prolong Gold Antifade Reagent (Invitrogen). Images were acquired using a Leica DM6000 upright confocal microscope equipped with a 63× oil immersion objective.

Animal studies: Crl:NU-*Foxn1^{nu}* mice (Charles Rivers Laboratories International, Inc., Wilmington, MA) were administered either 1×10^8 control S1MPs or SPION-loaded and capped S1MPs in PBS (100 μL) via a tail vein. At either 2 or 24 h post-injection, tissues were harvested, fixed in 10% formalin, and embedded in paraffin. Lung, spleen, and liver sections were deparaffinized and stained with Prussian blue and Nuclear Fast Red.[37] Briefly, tissues were deparaffinized in S3·Histo (BBC Biochemical) for 10 min, hydrated in decreasing solutions of aqueous ethanol, and stained with equal parts of 20% (v/v) hydrochloric acid and 10% (v/v) potassium ferrocyanide (Sigma–Alrich) for 20 min. Slides were then counterstained with Nuclear Fast Red (Sigma–Aldrich), and then dehydrated and cleared with S3 · Histo.

MTT cell proliferation assay: J774A.1 cells were seeded into 96-well plates at 5000 cells $well^{-1}$ in a final volume of 200 μL $well^{-1}$ complete medium. After 24 h, media (0.5 mL) containing oxidized S1MPs, either unloaded or loaded (electrostatic or capped) with SPIONs (10:1, S1MPs/cells), were added. After 24, 48, 72, and 96 h at 37 °C, the medium was removed and fresh medium containing MTT (0.5 mg mL^{-1}; Sigma) was added at 200 μL $well^{-1}$ for 4 h at 37 °C. The medium was then replaced with dimethyl sulfoxide (180 μL $well^{-1}$). After 30 min at room temperature, the absorbance was read at 570 nm using a SPECTRA max M2 plate reader (Molecular Devices).

Degradation studies: SPION-loaded S1MPs ($1–5 \times 10^6$), with and without the APTES cap, were suspended in PBS or FBS in microfuge tubes and rotated for up to 24 h at 25 or 37 °C using a Barnstead Thermodyne Labquake Rotator. At the indicated time points, S1MPs were either centrifuged or filtered (0.45 μm) to collect microparticles, and the supernatant and particle pellet were analyzed for iron and silicon content by ICP-OES using a Varian Vista AX instrument set at 1 kW, with plasma flow set to 15 L min^{-1}, auxiliary flow of 1.5 L min^{-1}, and a nebulizer flow of 0.75 L min^{-1}.

Data analysis: Data are presented as means and standard deviations, with at least three data points per group. For statistical comparison a Student's *t*-test was performed (two-tailed distribution, two-sample equal variance).

Acknowledgements

We thank Hitachi for training and use of the Hitachi S-5500 SEM instrument. We wish to thank Kenneth Dunner Jr. for TEM sample preparation and analysis (Figures 2 and 4) at the High-Resolution Imaging Facility at the University of Texas M. D. Anderson Cancer Center (MDACC). In the Department of Nanomedicine and Biomedical Engineering at the University of Texas Health Science Center we thank Sarah Amra for tissue processing and histological staining of specimens, Qingpo Li for particle injections in mice and tissue collection, and Matt Landry for assistance with image preparation. We wish to thank the ICMB and the MRC at the University of Texas at Austin for use of instrumentation and facilities. We thank Dwight Romanovicz and Hugo Celio at the University of Texas at Austin for help with STEM sample preparation and analysis. This research was supported by the Department of Defense, grants DODW81XWH-07-1-0596, DODW81XWH-09-1-0212, and DODW81XWH-07-2-0101; NASA NNJ06HE06A; NIH RO1CA128797; MDACC Institutional Core Grant #CA-016672; and State of Texas, Emerging Technology Fund.

[1] F. Giotta, V. Lorusso, E. Maiello, G. Filippelli, M. R. Valerio, M. Caruso, F. Verderame, A. Latorre, G. Colucci, *Ann. Oncol.* **2007**, *18* (Suppl 6), vi66–69.
[2] J. Treat, A. Greenspan, D. Forst, J. A. Sanchez, V. J. Ferrans, L. A. Potkul, P. V. Woolley, A. Rahman, *J. Natl. Cancer Inst.* **1990**, *82*, 1706–1710.
[3] A. Rahman, J. Treat, J. K. Roh, L. A. Potkul, W. G. Alvord, D. Forst, P. V. Woolley, *J. Clin. Oncol.* **1990**, *8*, 1093–1100.
[4] T. E. Stinchcombe, M. A. Socinski, C. B. Lee, D. N. Hayes, D. T. Moore, R. M. Goldberg, E. C. Dees, *J. Thorac. Oncol.* **2008**, *3*, 521–526.
[5] E. Tasciotti, X. Liu, R. Bhavane, K. Plant, A. D. Leonard, B. K. Price, M. M. Cheng, P. Decuzzi, J. M. Tour, F. Robertson, M. Ferrari, *Nat. Nanotechnol.* **2008**, *3*, 151–157.
[6] C. Chiappini, E. Tasciotti, J. R. Fakhoury, D. Fine, L. Pullan, Y. C. Wang, L. Fu, X. Liu, M. Ferrari, *ChemPhysChem* **2010**, *11*, 1029–1035.
[7] R. E. Serda, J. Gu, R. C. Bhavane, X. Liu, C. Chiappini, P. Decuzzi, M. Ferrari, *Biomaterials* **2009**, *30*, 2440–2448.
[8] P. Decuzzi, M. Ferrari, *Biomaterials* **2008**, *29*, 377–384.
[9] P. Decuzzi, S. Lee, B. Bhushan, M. Ferrari, *Ann. Biomed. Eng.* **2005**, *33*, 179–190.
[10] P. Decuzzi, R. Pasqualini, W. Arap, M. Ferrari, *Pharm. Res.* **2009**, *26*, 235–243.
[11] S. H. C. Anderson, H. Elliott, D. J. Wallis, L. T. Canham, J. J. Powell, *Phys. Status Solidi A* **2003**, *197*, 331–335.
[12] L. T. Canham, C. L. Reeves, J. P. Newey, M. R. Houlton, T. I. Cox, J. M. Buriak, M. P. Stewart, *Adv. Mater.* **1999**, *11*, 1505–1507.
[13] J. W. Smith, D. A. Cheresh, *J. Biol. Chem.* **1990**, *265*, 2168–2172.
[14] R. E. Serda, N. L. Adolphi, M. Bisoffi, L. O. Sillerud, *Mol. Imaging* **2007**, *6*, 277–288.
[15] X. Yang, H. Wang, D. W. Beasley, D. E. Volk, X. Zhao, B. A. Luxon, L. O. Lomas, N. K. Herzog, J. F. Aronson, A. D. Barrett, J. F. Leary, D. G. Gorenstein, *Ann. N. Y. Acad. Sci.* **2006**, *1082*, 116–119.
[16] J. R. Dorvee, M. J. Sailor, G. M. Miskelly, *Dalton Trans.* **2008**, 721–730.
[17] J. C. Thomas, C. Pacholski, M. J. Sailor, *Lab Chip* **2006**, *6*, 782–787.

[18] R. Weissleder, P. F. Hahn, D. D. Stark, E. Rummeny, S. Saini, J. Wittenberg, J. T. Ferrucci, *AJR Am. J. Roentgenol.* **1987**, *149*, 723–726.
[19] B. R. Bacon, D. D. Stark, C. H. Park, S. Saini, E. V. Groman, P. F. Hahn, C. C. Compton, J. T. Ferrucci, Jr., *J. Lab. Clin. Med.* **1987**, *110*, 164–171.
[20] R. Weissleder, D. D. Stark, B. L. Engelstad, B. R. Bacon, C. C. Compton, D. L. White, P. Jacobs, J. Lewis, *AJR Am. J. Roentgenol.* **1989**, *152*, 167–173.
[21] P. Reimer, T. Balzer, *Eur. Radiol.* **2003**, *13*, 1266–1276.
[22] A. Gabizon, H. Shmeeda, A. T. Horowitz, S. Zalipsky, *Adv. Drug Delivery Rev.* **2004**, *56*, 1177–1192.
[23] F. Gu, L. Zhang, B. A. Teply, N. Mann, A. Wang, A. F. Radovic-Moreno, R. Langer, O. C. Farokhzad, *Proc. Natl. Acad. Sci. USA* **2008**, *105*, 2586–2591.
[24] P. Decuzzi, M. Ferrari, *Biophys. J.* **2008**, *94*, 3790–3797.
[25] F. K. Swirski, M. Nahrendorf, M. Etzrodt, M. Wildgruber, V. Cortez-Retamozo, P. Panizzi, J. L. Figueiredo, R. H. Kohler, A. Chudnovskiy, P. Waterman, E. Aikawa, T. R. Mempel, P. Libby, R. Weissleder, M. J. Pittet, *Science* **2009**, *325*, 612–616.
[26] V. Manolova, A. Flace, M. Bauer, K. Schwarz, P. Saudan, M. F. Bachmann, *Eur. J. Immunol.* **2008**, *38*, 1404–1413.
[27] A. Beduneau, Z. Ma, C. B. Grotepas, A. Kabanov, B. E. Rabinow, N. Gong, R. L. Mosley, H. Dou, M. D. Boska, H. E. Gendelman, *PLoS ONE* **2009**, *4*, e4343.
[28] W. Liu, J. A. Frank, *Eur. J. Radiol.* **2009**, *70*, 258–264.
[29] T. Falguieres, P. P. Luyet, J. Gruenberg, *Exp. Cell Res.* **2009**, *315*, 1567–1573.
[30] B. Arkles, *Paint Coatings Int.* **2006**, *22*, 114.
[31] S. Fiorilli, P. Rivolo, E. Descrovi, C. Ricciardi, L. Pasquardini, L. Lunelli, L. Vanzetti, C. Pederzolli, B. Onida, E. Garrone, *J. Colloid Interface Sci.* **2008**, *321*, 235–241.
[32] R. E. Serda, S. Ferrati, B. Godin, E. Tasciotti, X. Liu, M. Ferrari, *Nanoscale* **2009**, *1*, 250–259.
[33] P. Decuzzi, B. Godin, T. Tanaka, S. Y. Lee, C. Chiappini, X. Liu, M. Ferrari, *J. Controlled Release* **2010**, *141*, 320–327
[34] X. Zhang, C. Zhang, H. Guo, W. Huang, T. Polenova, L. C. Francesconi, D. L. Akins, *J. Phys. Chem. B* **2005**, *109*, 19156–19160.
[35] S. Boujday, J. Blanchard, R. Villanneau, J. M. Krafft, C. Geantet, C. Louis, M. Breysse, A. Proust, *ChemPhysChem* **2007**, *8*, 2636–2642.
[36] R. Mellaerts, J. A. Jammaer, M. Van Speybroeck, H. Chen, J. Van Humbeeck, P. Augustijns, G. Van den Mooter, J. A. Martens, *Langmuir* **2008**, *24*, 8651–8659.
[37] A. K. Gupta, M. Gupta, *Biomaterials* **2005**, *26*, 1565–1573.

Received: January 27, 2010
Revised: April 2, 2010
Published online: May 31, 2010

